

Article

Study of the Contact Characteristics of Machine Tool Spindle Bearings under Strong Asymmetric Loads and High-Temperature Lubrication Oil

Yanfang Dong ^{1,2,3} , Feifan Chen ^{1,2}, Ming Qiu ^{1,2,*}, Huijie Wang ^{1,2} and Chuanmeng Yang ^{1,2,4}

- ¹ School of Mechatronics Engineering, Henan University of Science and Technology, Luoyang 471003, China
² Henan Provincial Cooperative Innovation Center for Advanced Manufacturing of Mechanical Equipment, Luoyang 471003, China
³ Hangzhou Bearing Test and Research Center Co., Ltd., Post-Doctoral Workstation, Hangzhou 310022, China
⁴ State Key Laboratory of Tribology, Tsinghua University, Beijing 100062, China
* Correspondence: qiuming69@126.com or qiuming@haust.edu.cn

Abstract: The contact characteristics of angular contact ball bearings are closely related to the thermal failure of high-speed spindle systems. This paper establishes a closed-loop iterative model for analyzing the ball–race contact characteristics of machine tool spindle bearings at different combined loads and oil supply temperatures, based on a five-degree-of-freedom quasi-static analysis model and the finite difference method. Additionally, the accuracy of the proposed model is verified by comparing the measured values of temperature rise with the predicted values. Based on the verification of the accuracy of the model, the contact characteristics of machine tool spindle bearings under strong asymmetric loads and high-temperature lubrication oil are discussed in detail. The results show that at elevated temperatures, the internal loads of angular contact ball bearings operating under combined loads become concentrated, which will lead to reduced fatigue life of the bearings and even thermal seizure.

Keywords: angular contact ball bearing; high temperature thermal effects; thermal–structural coupling; high speed spindle



Citation: Dong, Y.; Chen, F.; Qiu, M.; Wang, H.; Yang, C. Study of the Contact Characteristics of Machine Tool Spindle Bearings under Strong Asymmetric Loads and High-Temperature Lubrication Oil. *Lubricants* **2022**, *10*, 264. <https://doi.org/10.3390/lubricants10100264>

Received: 6 September 2022

Accepted: 13 October 2022

Published: 18 October 2022

Publisher's Note: MDPI stays neutral with regard to jurisdictional claims in published maps and institutional affiliations.



Copyright: © 2022 by the authors. Licensee MDPI, Basel, Switzerland. This article is an open access article distributed under the terms and conditions of the Creative Commons Attribution (CC BY) license (<https://creativecommons.org/licenses/by/4.0/>).

1. Introduction

The excess operating temperature of spindle bearings caused by the high-speed cutting directly affects the machining performance of precision machine tools. Furthermore, the thermal effects caused by high temperature rise are coupled with centrifugal effects and gyroscopic moments, affecting the performance of the bearing, and in severe cases, leading to thermal failure problems such as seizures and raceway burns [1]. Therefore, it is essential to model this complex thermal–structural coupling behavior and study the internal contact characteristics of the bearing during operation.

The fundamental of thermal analysis is the calculation of bearing heat generation. The most classic empirical model is proposed by Palmgren [2], but this model does not take into account the effect of high speed. Harris [3] also calculated the heat production of bearings more accurately by integrating the bearing dynamics; however, the calculation process is too complex to be practical. Therefore, most of the current research processed the calculation of bearing heat production based on quasi-static bearing mechanics. Li [4] analyzed the dynamic characteristics of bearings under combined loads based on a five-degree-of-freedom quasi-static model. Zhang [5,6] developed a five-degree-of-freedom analytical model considering the ball–raceway contact state with a new initial position assumption for investigating the dynamic characteristics of bearings under combined loads. These studies provide a detailed analysis of the influence of operating conditions on the internal load distribution, contact angle, and heat generation rate of bearings from

a mechanical point of view. Based on the analysis of the internal load distribution of the bearing, Zhang [7] investigated the thermal characteristics of bearings under high-speed grease lubrication conditions. Zhang [8] discussed the bearing thermal characteristics and considered the effect of thermal expansion of the bearing assembly under grease lubrication conditions. Yu [9] compared the dynamic characteristics of bearings with and without consideration of thermal expansion. However, the set-up conditions in these studies are relatively designated, since only the axial load is considered.

On the other hand, the bearing thermal characteristics analysis can be carried out on the basis of accurate calculation of heat generation. As an important method for the thermal analysis of bearings, the thermal network method is widely studied by scholars because of its efficiency and accuracy. Yan [10] proposed a network approach to the spindle bearing transient analysis, which considered the thermal–structural interactions. Zheng [11] proposed an enhanced nodal planning scheme, and an optimized thermal mesh model of a pair of front bearings mounted in a high-speed spindle was developed, also the structural constraints influences were introduced in a subsequent study [12]. Liu [13] introduced the temperature variation of the cooling system into a thermal resistance network model and analyzed the effect of cooling conditions on the temperature rise of the main components of the spindle system. Than [14] used the more efficient Runge-Kutta method to solve the non-linear thermal characteristics of high-speed spindle bearings based on the thermal network method. All these studies bring the thermal analysis of bearings closer to reality.

In recent years, with the continuous progress of science and technology, more and more scholars have started to study the performance of bearings under severe conditions. For example, Xia [15] studied the tribological behavior and vibration characteristics of full ceramic ball bearings under extreme working conditions such as cryogenics, heavy load, and oil-free lubrication. Wang [16] studied the influence of the thermal effect on the elasto-hydrodynamic lubrication performances of ball bearings and the vibration characteristics of bearings with defects under thermal elasto-hydrodynamic lubrication. Accordingly, the former analysis is basically carried out under single working conditions. However, in practical engineering applications, angular contact ball bearings inevitably have to work under extreme conditions. Therefore, the model for the bearings working under high speeds, high oil temperatures, and strong asymmetric loads is established in this paper. In the end, the influence of the high-temperature thermal effect on internal contact characteristics and fatigue life of bearings is studied in detail.

2. Analysis of the Mechanical Characteristics of Angular Contact Ball Bearings Considering Thermal Effects

For angular contact ball bearings, the additional forces caused by operation including centrifugal force, gyro moment, and thermal load direct impact the load distribution in the bearing and interact with the overall thermal characteristics of the system. At low and medium speeds, these loads caused by dynamic operation are very small and hardly react in the assessment of bearing performance. At high speeds, however, the bearing performance can be very sensitive to these additional forces. Therefore, a mathematical model is needed to describe the coupling characteristics of centrifugal force, gyro moment, and thermal load firstly.

2.1. Geometric Analysis

Figure 1a shows the internal geometric relationship of angular contact ball bearings. In the stationary state, the bearing inner and outer ring raceway curvature center O_i , O_o , and the center of the ball O are on the same line, this line and bearing radial plane between the angle is the initial contact angle α_0 , inner and outer ring groove curvature center between the distance A is

$$A = r_i + r_o - D_w = (f_o + f_i - 1) \cdot D_w = BD_w \quad (1)$$

where f_i and f_o are the inner and outer ring groove radius of curvature coefficient, r_i and r_o are the inner and outer raceway radius of curvature, respectively, D_w is the ball diameter.

$$r_p = d_m/2 + (r_i - D_w/2) \cdot \cos a_0 \tag{2}$$

where r_p is the radius of the inner ring raceway curvature center track, d_m is the bearing section circle diameter.

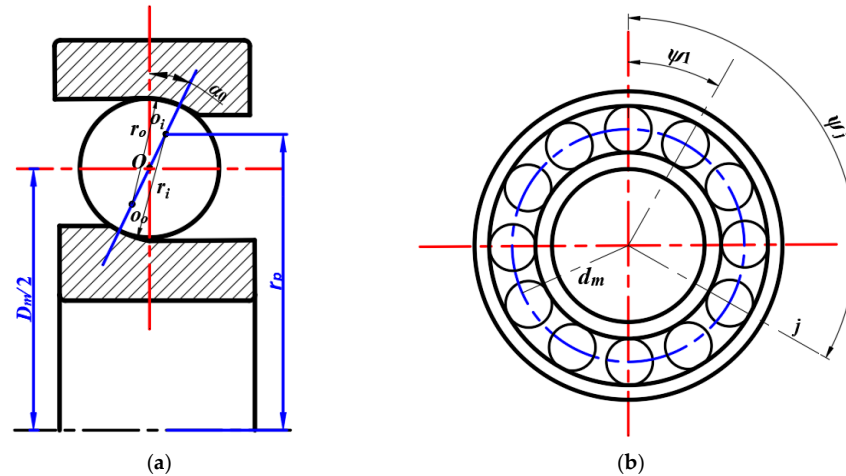


Figure 1. Angular contact ball bearing models. (a) Rolling bearing construction parameters; (b) the angular position of the ball.

Additionally, the azimuth angle ψ_j of the j th ball can be seen in Figure 1b, where Z is the number of balls.

$$\psi_j = 2\pi/Z \times (j - 1) \quad j = 1, 2, \dots, Z \tag{3}$$

The centrifugal force and gyroscopic moment generated during the operation of the bearing will make the center of curvature of the inner and outer raceway of the bearing not on a straight line. If the inner ring of the bearing is rotating and the outer ring is fixed, the center of curvature of the outer raceway is considered to be unchanged, but the position of the center of the steel ball and the center of curvature of the inner raceway changes from time to time. To facilitate the description of this change, a five-degree-of-freedom coordinate system located at the center of mass of the bearing is used to represent the movement of the inner ring. The vector $\{\delta\} = [\delta_x \delta_y \delta_z \theta_x \theta_y]^T$ represents the translational displacement in the three directions X , Y , and Z and the rotational displacement around the two directions X and Y . The corresponding load is $\{F\} = [F_x F_y F_z M_x M_y]^T$, as shown in Figure 2.

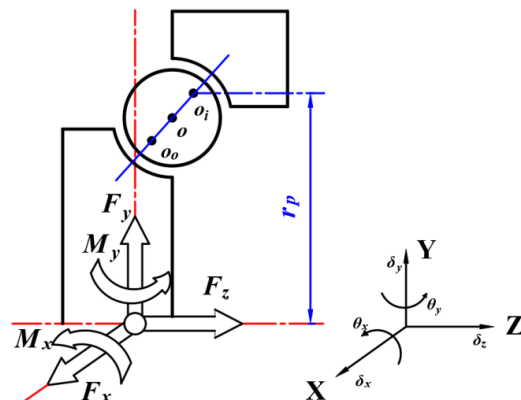


Figure 2. Angular contact ball bearing displacements and loads.

2.2. Deformation Analysis

2.2.1. Heat-Induced Deformation

The thermal expansion of the bearing components can be derived from the following equation, which is shown in Table 1

$$u = \vartheta \cdot \Delta T \cdot d \tag{4}$$

where ϑ is the coefficient of thermal expansion, ΔT is the temperature rise, d is the feature size.

Table 1. Equation for calculating the thermal expansion of bearing components.

Deformation Components	Calculation Formula
Thermal expansion of the ball	$\epsilon_b = \vartheta_b \cdot \Delta T_b \cdot D_w / 2$
Radial heat deformation of the inner ring considering the thermal effect of the shaft and inner ring	$\epsilon_{ir} = \vartheta_i \cdot \Delta T_i \cdot d_i + [\vartheta_s \cdot \Delta T_s \cdot (1 + \nu_s) - \vartheta_i \cdot \Delta T_i] d_i^2 / d_{ig}$
Thermal expansion of the outer ring considering the outer ring limit of the bearing housing	$\epsilon_{or} = \vartheta_h \cdot \Delta T_h \cdot (1 + \nu_h) d_{og}$

In Table 1, b, s, h for ball, spindle, and housing, respectively, ν is the Poisson’s ratio.

- (1) Displacement due to thermal expansion of the outer ring

As shown in Figure 3a, the radial expansion along the direction of normal contact is

$$\epsilon_{orn} = \epsilon_{or} \cos a_o \tag{5}$$

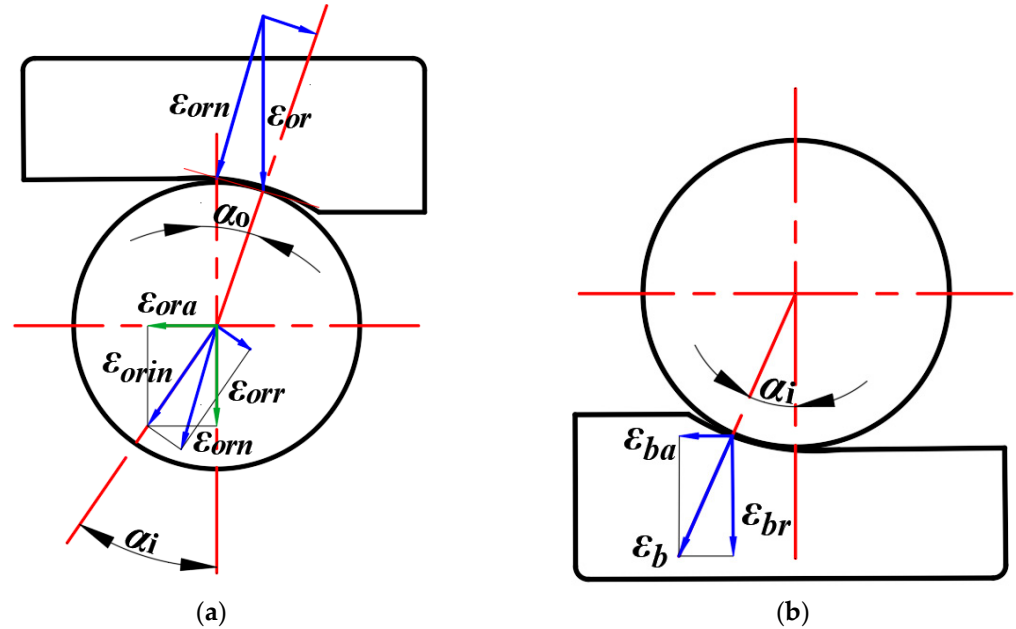


Figure 3. Thermal displacement between ball and ring. (a) Ball with outer ring; (b) ball with inner ring.

So, the displacement of the ball in the direction of contact is

$$\epsilon_{orin} = \epsilon_{orn} \cos(a_i - a_o) \tag{6}$$

Therefore, the radial and axial displacement of the bearing caused by the thermal expansion of the outer ring is

$$\begin{cases} \varepsilon_{orr} = \varepsilon_{orin} \cos a_i \\ \varepsilon_{ora} = \varepsilon_{orin} \sin a_i \end{cases} \quad (7)$$

(2) Displacement due to thermal expansion of the ball

As shown in Figure 3b, the radial and axial displacement of the bearing caused by the thermal expansion of the ball is

$$\begin{cases} \varepsilon_{br} = \varepsilon_b \cos a_i \\ \varepsilon_{ba} = \varepsilon_b \sin a_i \end{cases} \quad (8)$$

2.2.2. Centrifugal Deformation

The centrifugal expansion of the inner ring and shaft can be obtained from Timoshenko’s equation for the expansion of a rotating disc

$$u_{cent} = \frac{\rho\omega^2}{32E} d_m [d_{si}^2(3 + \nu) + d_m^2(1 - \nu)] \quad (9)$$

where E is the modulus of elasticity, ω is the rotational speed, ρ is the radius of the groove center, and ν is the Poisson’s ratio.

Considering the above factors together, the deformation relationship between the center of the ball and the center of curvature of the inner and outer ring raceway can be obtained, as shown in Figure 4. Where O' , O'_i represents the position of the center of the ball and the center of curvature of the inner ring raceway after deformation; l_{ij} and l_{oj} represent the distance between the center of the j th ball and the center of curvature of the inner and outer ring raceway after deformation; B_{aj} and B_{rj} represent the axial and radial deformation displacement of the center of curvature of the inner ring raceway at the position of the j th ball; δ_{ij} and δ_{oj} represent the contact deformation between the j th steel ball and the inner and outer ring; a_{ij} and a_{oj} represent the contact angle between the ball and the inner and outer raceway, respectively; A_{aj} and A_{rj} represent the axial and radial distance between the inner raceway curvature center and the outer raceway curvature center after deformation; X_{aj} and X_{rj} represent the axial and radial distance between the ball center and the outer raceway curvature center after deformation. From these geometric relationships, the following expressions can be obtained

$$\begin{aligned} l_{ij} &= (f_i - 0.5) \cdot (D_w + \varepsilon_b) + \delta_{ij} \\ l_{oj} &= (f_o - 0.5) \cdot (D_w + \varepsilon_b) + \delta_{oj} \end{aligned} \quad (10)$$

$$\begin{aligned} B_{aj} &= \delta_z + r_p(\theta_x \cos \psi_j - \theta_y \sin \psi_j) + \varepsilon_{ba} + \varepsilon_{ora} \\ B_{rj} &= \delta_x \sin \psi_j + \delta_y \cos \psi_j + \varepsilon_{ir} + u_{cent} - \varepsilon_{br} - \varepsilon_{orr} \end{aligned} \quad (11)$$

$$\begin{aligned} A_{aj} &= A \cdot \sin a_0 + B_{aj} \\ A_{rj} &= A \cdot \cos a_0 + B_{rj} \end{aligned} \quad (12)$$

$$\begin{aligned} \sin a_{ij} &= \frac{A_{aj} - X_{aj}}{l_{ij}} & \sin a_{oj} &= \frac{X_{aj}}{l_{oj}} \\ \cos a_{ij} &= \frac{A_{rj} - X_{rj}}{l_{ij}} & \cos a_{oj} &= \frac{X_{rj}}{l_{oj}} \end{aligned} \quad (13)$$

Then, by Pythagoras’ theorem, we have

$$\begin{aligned} (A_{aj} - X_{aj})^2 + (A_{rj} - X_{rj})^2 - l_{ij}^2 &= 0 \\ X_{aj}^2 + X_{rj}^2 - l_{oj}^2 &= 0 \end{aligned} \quad (14)$$

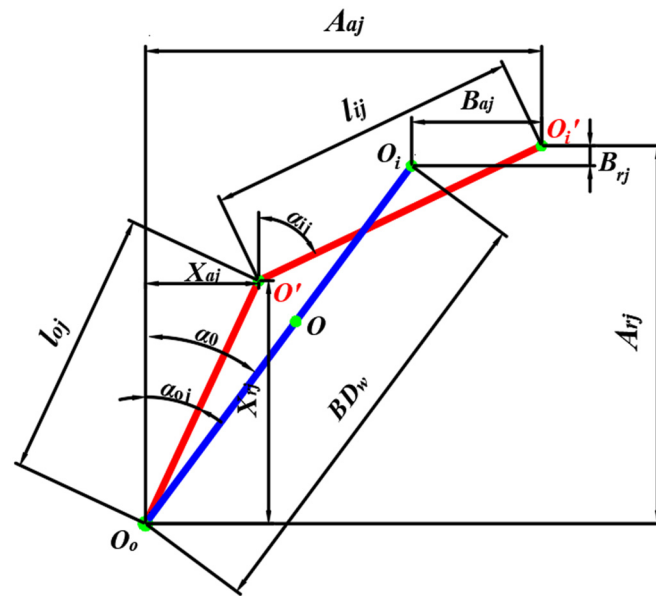


Figure 4. Deformation of the ball center in relation to the center of curvature of the inner and outer ring raceways.

2.3. Force Analysis

When the ball and raceway are in contact, the ball of the high-speed bearing is not only subject to the force of the inner and outer raceway, but also to the gyroscopic moment and centrifugal force. Figure 5a is the force analysis of the ball in this case.

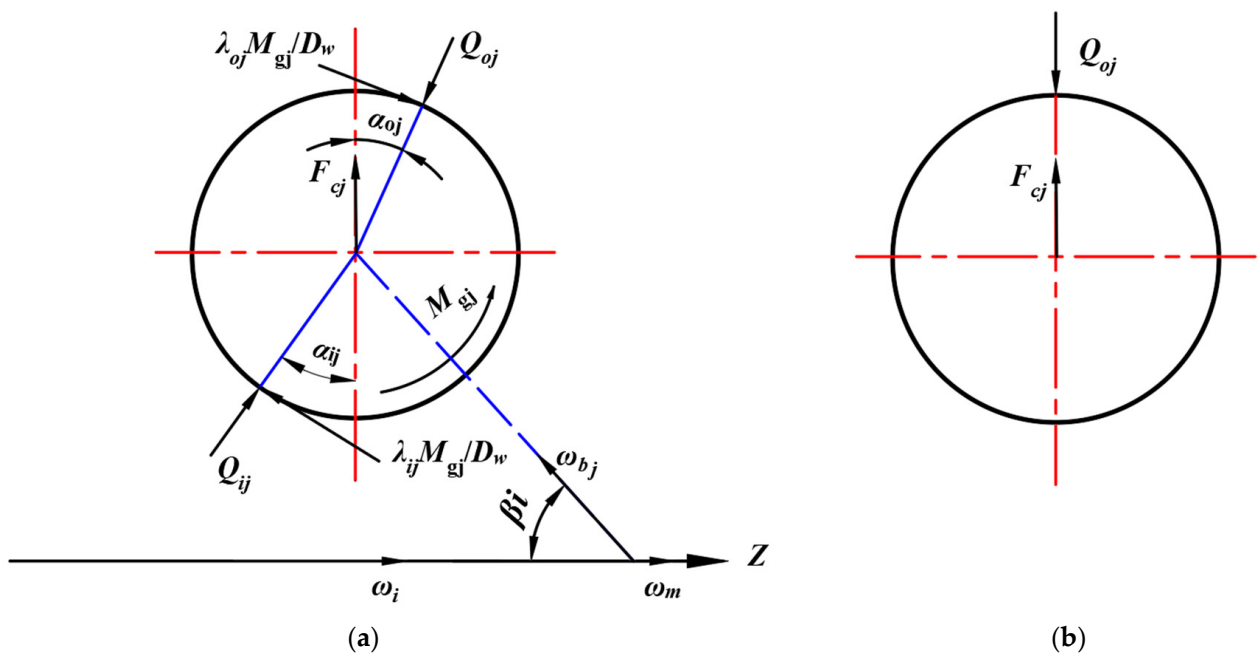


Figure 5. Force analysis of the ball. (a) Ball and raceway contact; (b) ball and raceway separation.

The equation of equilibrium of the force on the ball at this point is as follows

$$\begin{aligned}
 Q_{ij} \sin a_{ij} - Q_{oj} \sin a_{oj} - \frac{M_{gj}}{D_w} (\lambda_{ij} \cos a_{ij} - \lambda_{oj} \cos a_{oj}) &= 0 \\
 Q_{ij} \cos a_{ij} - Q_{oj} \cos a_{oj} - \frac{M_{gj}}{D_w} (\lambda_{ij} \sin a_{ij} - \lambda_{oj} \sin a_{oj}) + F_{cj} &= 0
 \end{aligned}
 \tag{15}$$

where λ_{ij} and λ_{oj} represents the inner and outer ring raceway control parameters, its value can be referred to the literature [3], this paper uses the outer ring raceway control, $\lambda_{ij} = 0$, $\lambda_{oj} = 2$; Q_{ij} and Q_{oj} represents the contact force between the ball and the inner and outer ring raceway, the following formula calculation

$$\begin{cases} Q_{ij} = K_{ij}\delta_{ij}^{1.5} \\ Q_{oj} = K_{oj}\delta_{oj}^{1.5} \end{cases} \quad (16)$$

where K_{ij} and K_{oj} represent the load deformation constants between the j th ball and the inner and outer rings, for the calculation of the contact deformation δ refer to the literature [17].

In addition, the centrifugal force F_{cj} and the gyroscopic moment M_{gj} of the ball can be expressed as

$$F_{cj} = \frac{1}{2}md_m\omega_{mj}^2 \quad (17)$$

$$M_{gj} = J\omega_{mj}\omega_{bj} \sin \beta_j \quad (18)$$

where m and J represent the mass and rotational inertia of the ball; ω_{mj} and ω_{bj} represent the angular velocity of the ball's revolution and rotation, which can be calculated from the following equation by assuming no macroscopic sliding in the contact zone [18]

$$\begin{aligned} \omega_{mj} &= \frac{\omega_i(1-\gamma_{ij})\cos(a_{oj}-\beta_j)}{(1+\gamma_{oj})\cos(a_{ij}-\beta_j)+(1-\gamma_{ij})\cos(a_{oj}-\beta_j)} \\ \omega_{bj} &= \frac{d_m}{D_w} \frac{\omega_i(1-\gamma_{ij})(1+\gamma_{oj})}{(1+\gamma_{oj})\cos(a_{ij}-\beta_j)+(1-\gamma_{ij})\cos(a_{oj}-\beta_j)} \end{aligned} \quad (19)$$

The attitude angle β_j is determined according to D'Alembert's principle.

$$\tan \beta_j = \frac{M(N+1)\sin a_{ij} + 2\sin a_{oj}}{M(N+1)\cos a_{ij} + 2(\cos a_{oj} + D_w/d_m) + G} \quad (20)$$

$$\begin{cases} M = \frac{Q_{ij}a_{ij}L_{ij}}{Q_{oj}a_{oj}L_{oj}} \\ G = \frac{D_w}{d_m}M[\cos(a_{ij} - a_{oj}) - N] \\ N = \frac{1+D_w/d_m \cos a_{oj}}{1-\cos a_{ij}} \end{cases} \quad (21)$$

where a_{ij} and a_{oj} represent the semi-long axis of the ellipse of ball contact with the inner and outer raceway; L_{ij} and L_{oj} represent the second type of elliptic integral of ball contact with the inner and outer raceway.

Then, the case where the ball is separated from the inner raceway is discussed. It can find the judgment criterion of contact state between ball and raceway in references [5,6]. That is, the sum of deformations of the inner and outer ring δ_n^k is less than 0, the ball and raceway are separated, as shown in Equation (22).

$$\delta_n^k \equiv \overline{O'_i O_o} - O_i O_o \quad (22)$$

Due to the action of centrifugal force, the separation of the ball from the raceway can only occur on the inner raceway, at this time the ball under the action of centrifugal force along the outer raceway is "climbing", until the ball and the outer raceway is vertical contact to reach a new equilibrium state [6], at this time the steel ball force as shown in Figure 5b, this state of the ball and the inner raceway separation, its rotation and the direction of common line, the gyroscopic moment is zero, so the ball force equilibrium equation becomes

$$\begin{cases} Q_{ij} = 0 \\ Q_{oj} = F_{cj} \end{cases} \quad (23)$$

In summary, a global mechanical analysis of the inner ring of the bearing, based on a local ball analysis, leads to

$$\left\{ \begin{aligned} F_x &= \sum_{j=1}^Z \left(Q_{ij} \cos a_{ij} + \frac{\lambda_{ij} M_{gj}}{D_w} \sin a_{ij} \right) \sin \psi_j \\ F_y &= \sum_{j=1}^Z \left(Q_{ij} \cos a_{ij} + \frac{\lambda_{ij} M_{gj}}{D_w} \sin a_{ij} \right) \cos \psi_j \\ F_z &= \sum_{j=1}^Z \left(Q_{ij} \sin a_{ij} - \frac{\lambda_{ij} M_{gj}}{D_w} \cos a_{ij} \right) \\ M_x &= \sum_{j=1}^Z \left(Q_{ij} \sin a_{ij} - \frac{\lambda_{ij} M_{gj}}{D_w} \cos a_{ij} \right) r_p \cos \psi_j \\ M_y &= \sum_{j=1}^Z \left(Q_{ij} \sin a_{ij} - \frac{\lambda_{ij} M_{gj}}{D_w} \cos a_{ij} \right) r_p \sin \psi_j \end{aligned} \right. \quad (24)$$

The dynamic characteristics of the bearing considering thermal effects can be obtained by solving the above set of equations in conjunction with the displacement coordination equation and the equilibrium equation for the force on the ball.

3. Thermal Analysis of Spindle Bearing Systems

3.1. Heat Balance Equation and Nodes Planning

In this paper, the thermal network method is also used to calculate the temperature of the spindle bearing system. The model is based on the spindle system shown in Figure 6, and the thermal nodes arranged in accordance with the structural characteristics of this system are shown in Figure 6. Nodes 46 and 47 represent the ambient and oil temperatures, respectively, while the temperature of node 48 is assumed to be approximately equal to the oil temperature and the temperature of node 49 to be approximately equal to the ambient temperature for ease of solution due to the difficulty of monitoring the temperature inside the box. The material physical parameters of the spindle-related components are shown in Table 2.

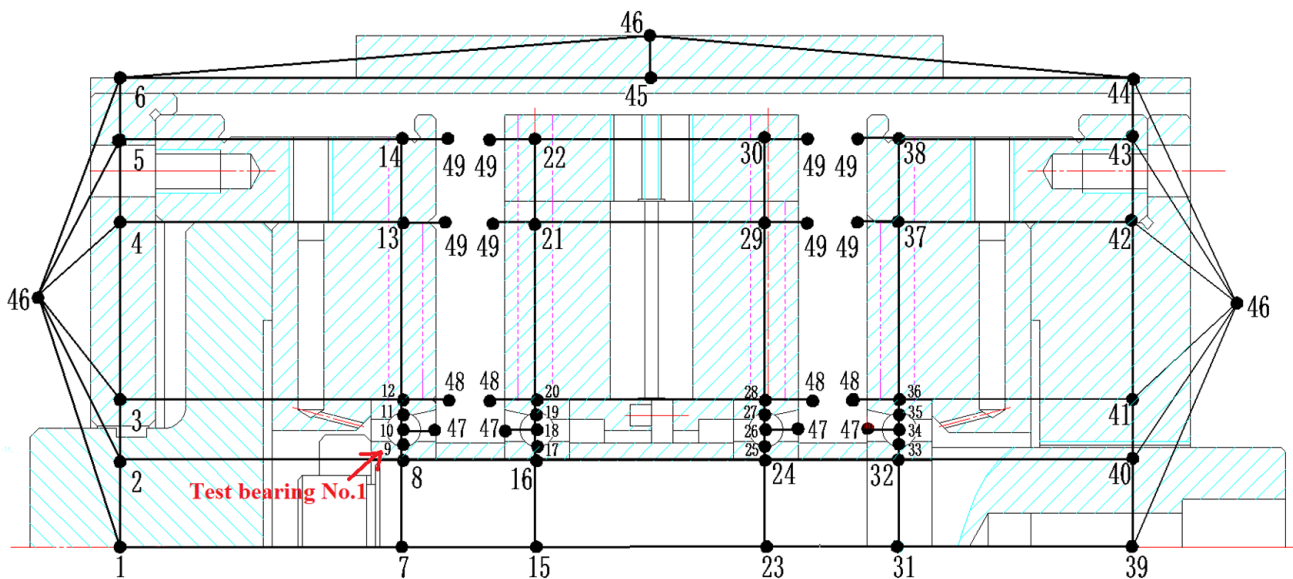


Figure 6. Schematic diagram of the spindle system structure and thermal node arrangement.

Table 2. Material properties.

Materials	Density (kg/m ³)	Coefficient of Thermal Expansion (μm/(°C))	Young's Elastic Modulus (GPa)	Poisson's Ratio	Thermal Conductivity (W/(m · K))	Specific Heat Capacity (J/(kg · °C))
45#steel	7850	11.6	206	0.26	50.2	486
GCr15	7810	12.5	219	0.3	40.1	450
40Cr	7900	15.5	211	0.28	66.6	460

Assuming that each thermal node is linked to other nodes through thermal resistances $R_{a,b}$, where a and b are the indexes of the linked nodes, the following heat balance equation is established for each node in Figure 6, according to Kirchhoff's law and the law of conservation of energy

$$\sum_{b=1}^n \frac{T_b - T_a}{R_{a,b}} + Q_a = m_a C_a \frac{\partial T_a}{\partial t}, \quad b = 1, 2, 3, \dots, n \quad (25)$$

where T is the node temperature; m is the node mass; C is the specific heat capacity; Q is the heat generated per unit time at node a; and the number of nodes $n = 49$.

The matrix form of the set of heat balance equations for the entire heat transfer system created from Equation (25) is

$$[R][T] + [C][\dot{T}] = [Q] \quad (26)$$

where $[R]$ is the thermal resistance coefficient matrix, $[C]$ is the heat capacity matrix, $[Q]$ is the heat flow matrix, and $[T]$ is the node temperature matrix.

3.2. Heat Generation

The research object of this paper is a mechanical spindle, the main source of heat that is the frictional heat of the bearing, and angular contact ball bearings in the following forms of frictional torque mainly exist.

- (1) Frictional torque M_1 due to elastic hysteresis

$$M_1 = 0.25d_m(1 - \gamma^2) \sum_{j=1}^Z (\varphi_{oj} + \varphi_{ij})\beta \quad (27)$$

- (2) Frictional torque M_2 due to differential sliding

$$M_2 = 0.5d_m(1 - \gamma^2) / D_w \cdot \sum_{j=1}^Z (M_{2ij} + M_{2oj})f_s \quad (28)$$

- (3) Frictional torque M_3 due to spin-slip

$$M_{3i(o)} = \frac{3}{8}f_s \sum_{j=1}^Z (Q_{i(o)j} a_{i(o)j} L_{i(o)j}) \quad (29)$$

- (4) Frictional torque M_4 caused by contact between ball and cage

$$M_4 = 0.5D_w f_c Q_c \quad (30)$$

- (5) Viscous friction torque M_5 of the lubricant

$$M_5 = 6.53\alpha_{oil}^{-1} S \left(\frac{d_m}{2} \right) \sum_{j=1}^Z \left[\left(\frac{h_o + h_i}{2} \right) (a_{ij} + a_{oj}) \right] \quad (31)$$

where β is the elastic hysteresis coefficient; f_s is the sliding friction coefficient between ball and raceway; W_{eb} is the cage weight; f_c is the sliding friction coefficient between ball and cage; a_{oil} is the lubricant viscous pressure coefficient; S is the lubrication adequacy coefficient; $h_{i(o)}$ is the oil film thickness; $\varphi_{i(o)j}$, $M_{2i(o)j}$ are calculated in detail with reference to the literature [19]. The friction torque results for the closed-loop iterations are shown in Figure 7.

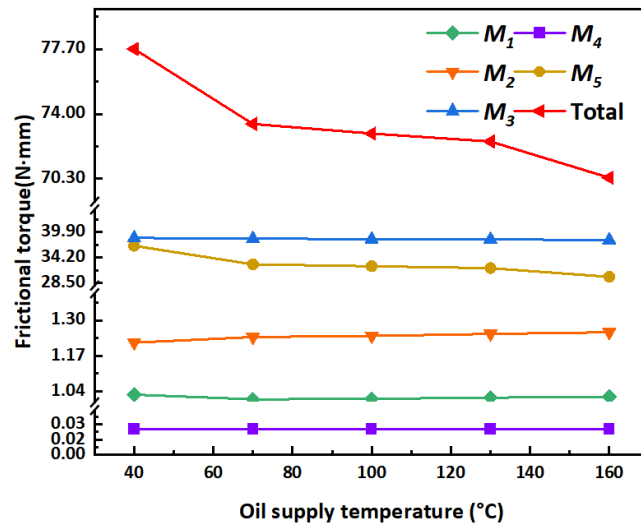


Figure 7. Frictional torque calculation results.

Bearing heat generation is calculated according to the following formula

$$W = \omega \cdot M \quad (32)$$

where ω is the angular velocity, M is the frictional torque and W is the power loss.

3.3. Heat Transfer Analysis

The temperature of the spindle system is influenced not only by the heat generated by the bearings, but also by the heat transfer from the system (heat conduction and heat convection), mainly in the following areas.

- (1) Heat conduction between the inner ring of the bearing and the shaft
- (2) Heat conduction between the ball and the inner and outer rings of the bearing
- (3) Heat conduction between bearing outer ring and housing
- (4) Heat conduction between bearing housing and spindle housing
- (5) Natural convection between spindle housing, end caps, etc., and ambient air
- (6) Forced convection between high-speed rotating surfaces and air in the system
- (7) Forced convection between the sides of high-speed rotating surfaces and air
- (8) Forced convection of coolant, lubricant, and flow-through surfaces

The thermal conductivity thermal resistance and convective thermal resistance for a one-dimensional steady-state heat transfer process are calculated as

$$\begin{aligned} R &= L_d / \lambda A_m \\ R_h &= 1 / h A_m \end{aligned} \quad (33)$$

where λ is the thermal conductivity of the material; L_d is the characteristic length of thermal conductivity; A_m is the heat transfer area; h is the convective heat transfer coefficient. The radial and axial thermal resistance between the nodes can be obtained by simplifying the inner and outer rings of the bearing, the shaft, etc., to a hollow cylinder.

In addition, the convective heat transfer coefficient is

$$h = Nu \cdot \lambda_{air} / d_e \tag{34}$$

where λ_{air} is the air thermal conductivity; d_e is the convective heat transfer characteristic length; Nu is the Nussle number, which can be found in Table 3.

Table 3. Thermal contact resistance and convective characteristic parameters.

Models	Applications	Comment
$Nu = \left\{ 0.6 + \frac{0.387(Re)^{1/6}}{\left[1 + (0.559/Pr)^{9/16}\right]^{8/27}} \right\}$	Natural convection between the bearing housing and the air [11]	Re—Reynolds number Pr—Prandtl number N—Spindle speed
$Nu = \left\{ 0.825 + \frac{0.387(Re)^{1/6}}{\left[1 + (0.492/Pr)^{9/16}\right]^{8/27}} \right\}$	Natural convection between housing, end caps, etc., and ambient air [11]	L_g —Thickness of the void space between the two contact surfaces
$Nu = 0.119Re^{2/3} \quad 800 \leq Re \leq 10^5$	Forced convection between rotating surfaces and air [20]	h_{ring} —Outer ring thickness S_{o-z} —Contact surface area between outer ring and bearing housing
$\begin{cases} Nu = 0.4\sqrt{Re}Pr^{1/3} & Re < 2.5 \times 10^5 \\ Nu = 0.238Re^{0.8}Pr^{0.6} & Re > 3.2 \times 10^5 \end{cases}$	Forced convection between the sides of the rotating surface and the air [11]	h_{gap} —Initial clearance T_{ring} —Outer ring temperature T_h —Bearing housing temperature
$h = 0.0986 \left\{ \frac{N}{v_{oil}} \left[1 - \frac{\gamma}{d_m} \right] \right\}^{0.5} kPr^{1/3}$	Average convective heat transfer coefficient between the lubricant and the original components in the bearing [21]	r_h —Inner radius of bearing housing h_{cont} —Contact conductivity e —Elliptical eccentricity
$R_{c1} = \frac{1}{\pi \lambda_{ring}} \left(\frac{E_e(e_i, \pi/2)}{a_i} + \frac{E_e(e_o, \pi/2)}{a_o} \right)$	Thermal contact resistance between ball and raceway [13]	A_{i-s} —Contact area between shaft and inner ring E_e —First class elliptic integrals
$R_{c1} = \frac{1}{A_{i-s} h_{cont}} = \frac{L_g (\lambda_{ring} + \lambda_s)}{2 A_{i-s} A_r^* \lambda_{ring} \lambda_s}$	Thermal contact resistance between the shaft and the inner ring of the bearing [11]	A_r^* —Dimensionless actual contact area v_{oil} —Lubricant kinematic viscosity
$R_{c3} = \frac{h_{ring}}{\lambda_{ring} S_{o-z}} + \frac{h_{gap} - (T_{ring} - T_h) \cdot \partial_o \cdot r_h}{\lambda_{air} S_{o-z}}$	Thermal contact resistance between outer ring and bearing housing [14]	λ_s —Thermal conductivity of spindle materials

Based on the analysis in Sections 2 and 3, the general steps of the nonlinear bearing thermal analysis algorithm proposed in this paper can be obtained, as shown in Figure 8.

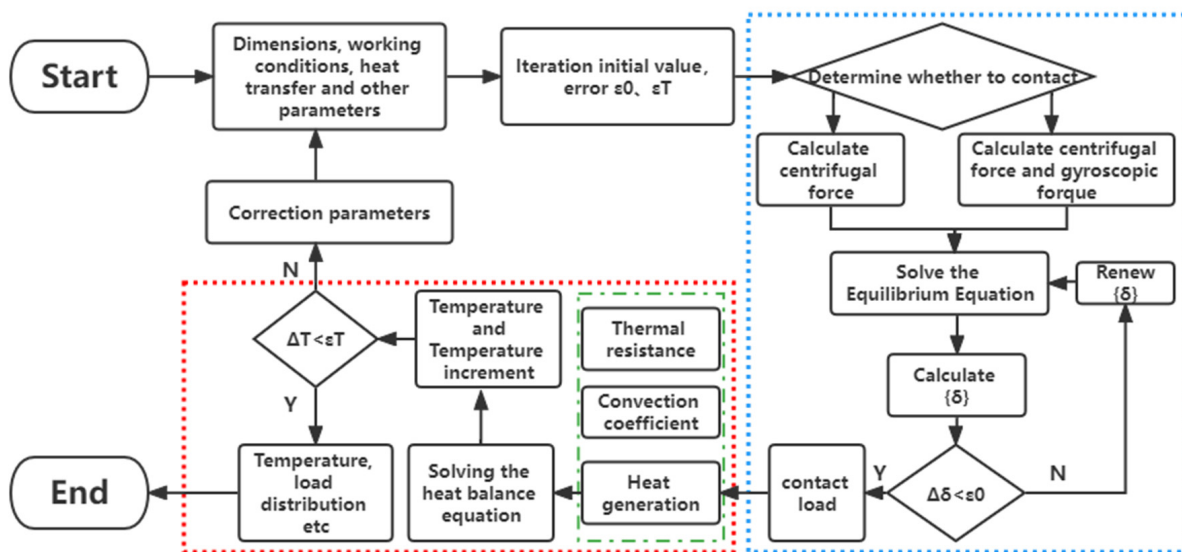


Figure 8. Closed-loop iterative process.

4. Experiment

In order to verify the correctness of the thermal–structural coupling model proposed above, a bearing high-temperature high-speed testing machine as shown in Figure 9 was built. The rotating speed range of the test machine is 2000–36,000 rpm, and the oil supply temperature can be adjusted from room temperature to 180 °C. All tests are performed in a laboratory with a controlled ambient temperature of 32–34 °C.

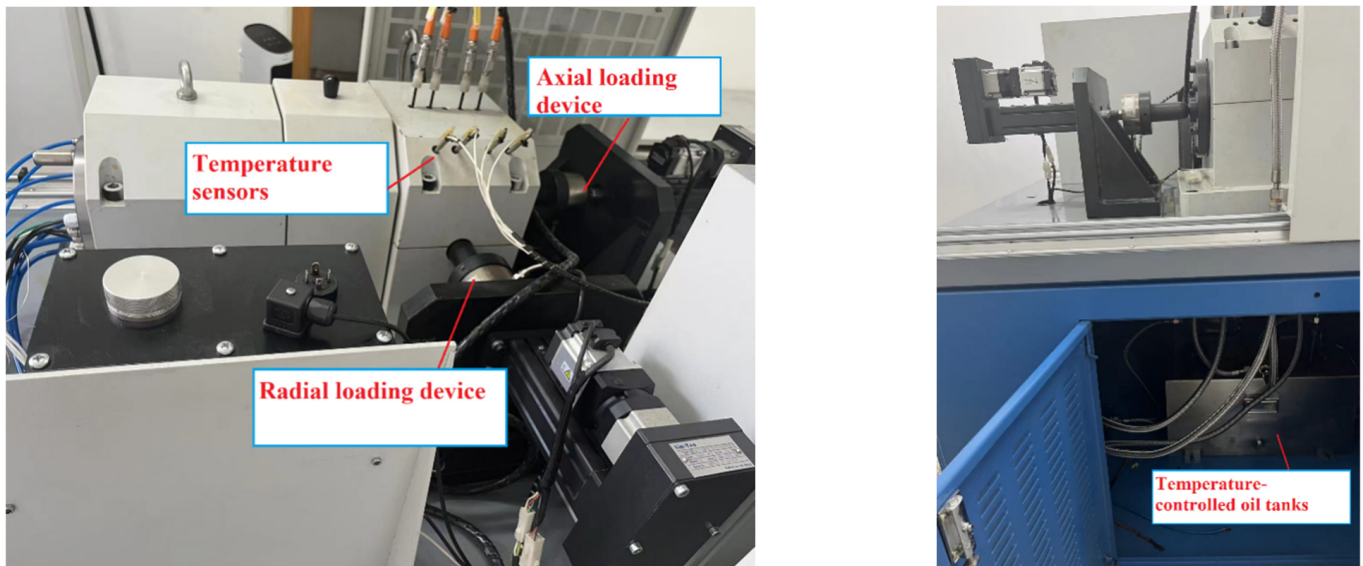


Figure 9. Test rig.

The bearing parameters used for the test are shown in Table 4. The 4050 aviation lubricant (−40 °C–203 °C) was used as the lubricant. Temperature measurements were recorded on the computer at 0.1 s intervals. The test is continued until the thermal steady state condition is stopped and allowed to cool to room temperature before the next set of tests is carried out.

Table 4. Basic structural parameters of angular contact ball bearing 7008.

Parameter Type	Value
Pitch diameter of the bearing d_m /mm	54.007
Number of balls	19
Ball diameter D_w /mm	7.144
Contact angle	15
Radius of curvature of the inner raceway r_i /mm	4
Radius of curvature of the outer raceway r_o /mm	3.79
Inner raceway diameter d_{ig} /mm	46.838
Outer raceway diameter d_{og} /mm	61.176

In practical applications, strong asymmetric loads (pure radial loads or combined loads under small axial forces) and high rotational speeds [6] can cause the balls to disengage from the inner raceway. Therefore, the test conditions were set to an axial load of 100 N, a radial load of 900 N, and a rotational speed of 12,000 rpm. Simulate bearing operation at different temperatures by controlling the oil supply temperature (heating the oil to the desired temperature before the spindle rotates).

5. Discussion

5.1. Validation

The test temperature of the outer surface of the outer ring of the test bearing No. 1 (given in Figure 6) was compared with the calculated results, and the results are shown in Figure 10. It can be seen that the accuracy of the steady-state results is good, with a maximum deviation of only 3%. The transient prediction is initially deviated, which is because the speed is stepped loaded during the test, and the change in spindle speed will change the oil temperature and convection intensity, but the speed and oil temperature of the prediction model are ideal values, so this error is within the allowable range. It is easy to see that the proposed model has a high accuracy, which means that it can be used for the prediction of other parameters.

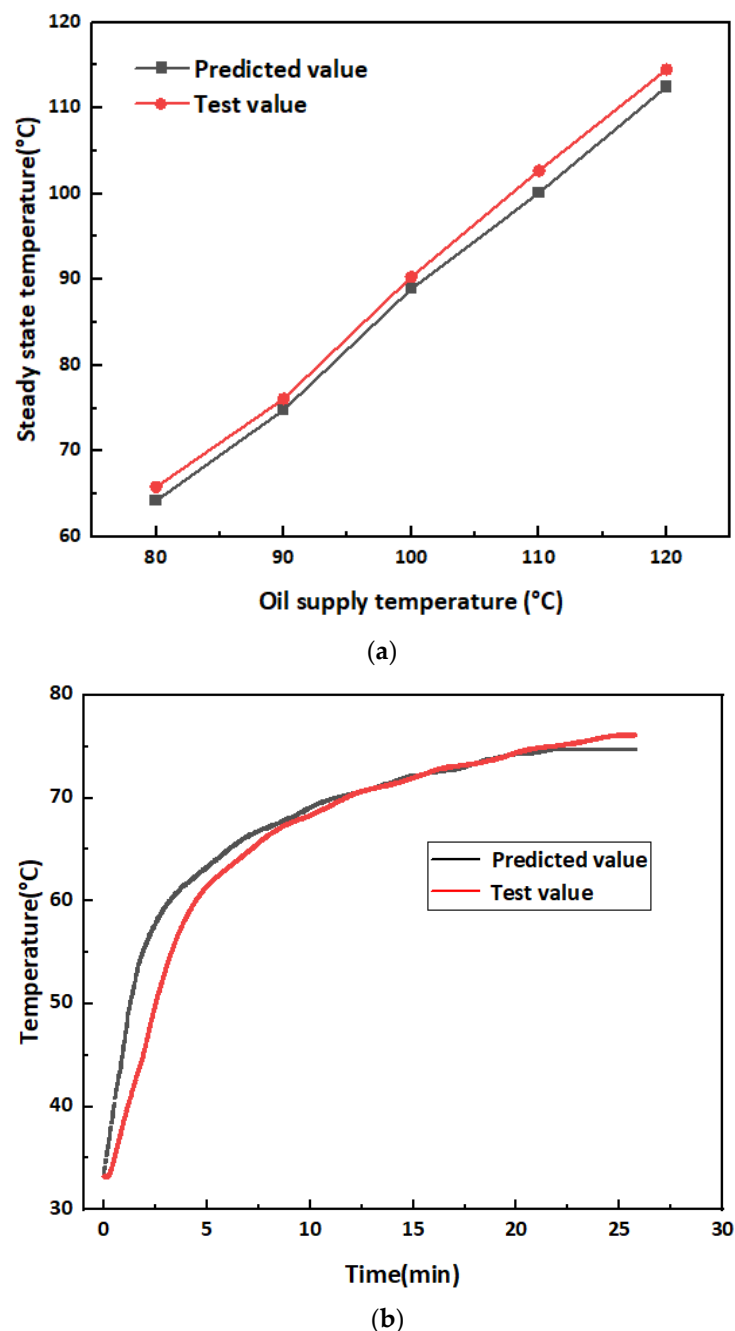


Figure 10. Comparison of results. (a) Comparison of steady state results; (b) comparison of transient results at supply oil temperature 90 °C.

5.2. Effect of Temperature on Contact Characteristics

As shown in Figure 11, at the same speed and load, the temperature rise will increase the maximum contact force inside the bearing, which is obviously caused by thermal expansion. Meanwhile, at a temperature difference of 100 °C, the contact force between the ball and the inner and outer raceways increases by about 8%, which also shows that the thermal effect has a relatively huge impact on the contact force relative to the speed and load. In addition, it can be seen in Figure 11b that the thermal effect will change the contact state of the ball and the raceway.

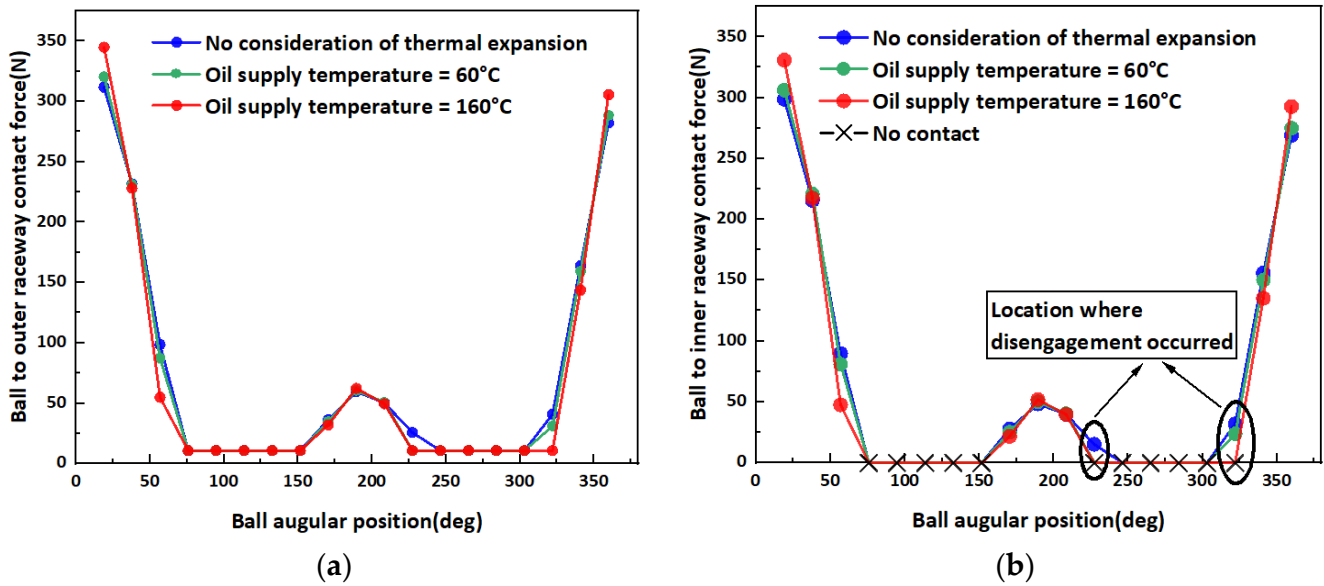


Figure 11. Ball and raceway contact forces. (a) Ball to outer raceway; (b) Ball to inner raceway.

Figure 12 illustrates the contact characteristics between the balls and raceways in the load zone. It can be seen that the contact force in the light load region and the heavy load region tends to be concentrated with the increase in the bearing operating temperature.

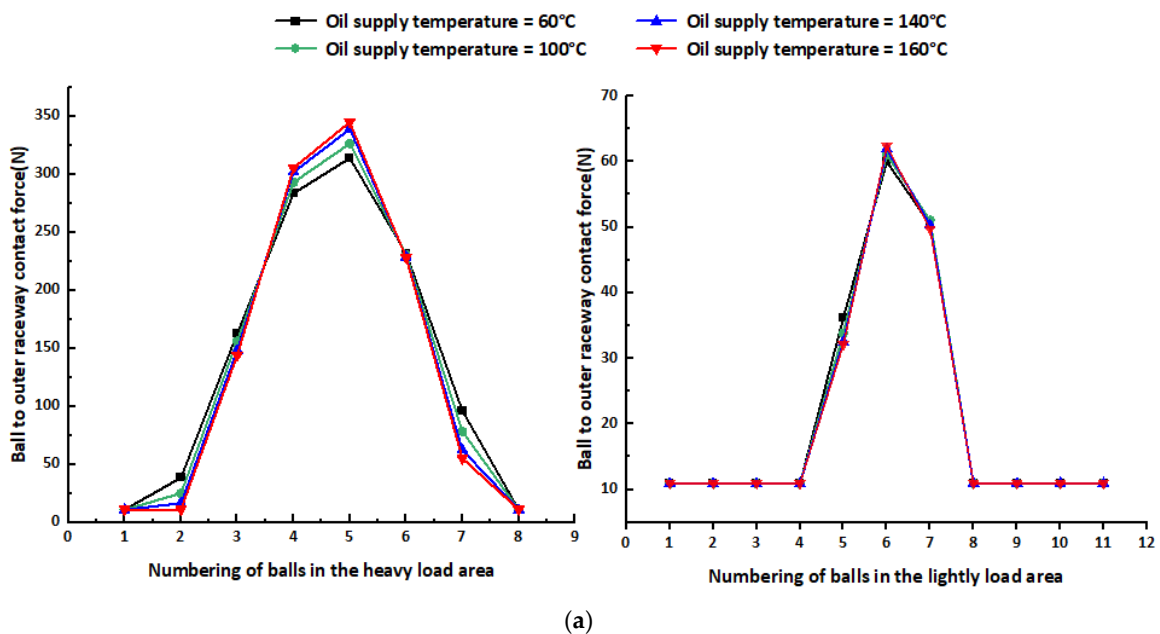


Figure 12. Cont.

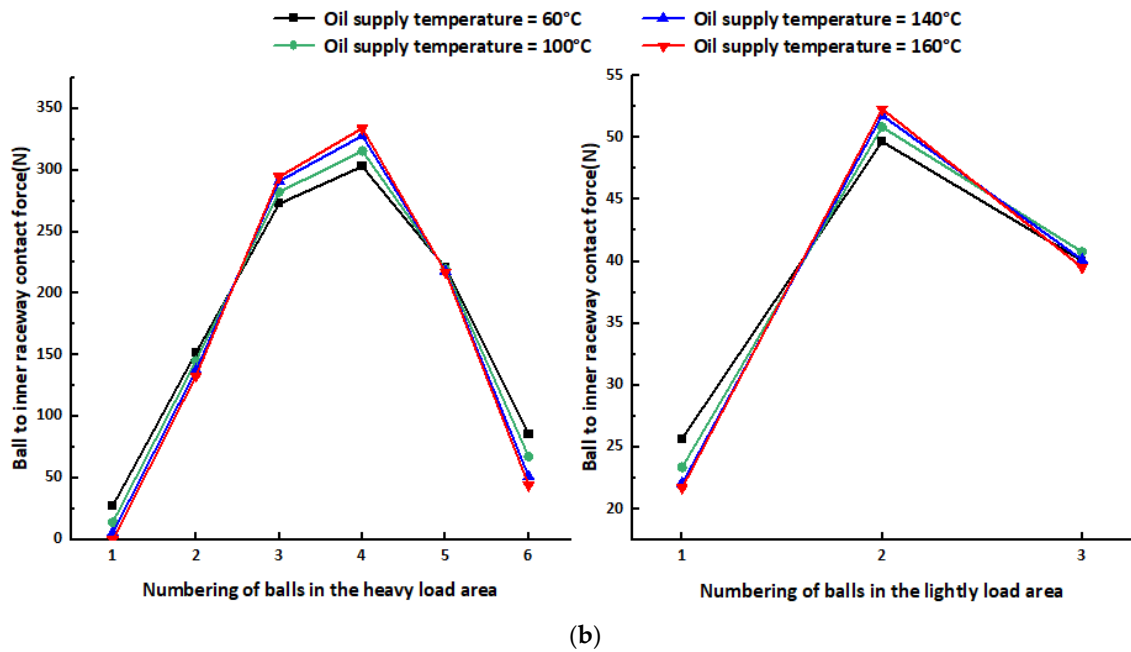


Figure 12. Variation of contact force in the loaded area. (a) Ball and outer raceway; (b) ball and inner raceway.

In fact, these phenomena are even more evident in the variation of contact angles, as shown in Figure 13. As the working temperature increases, the number of balls in the inner contact zone decreases, the number of balls with a contact angle of 0 degrees in the outer contact zone increases and the contact angle between the balls and both the inner and outer raceways increases, which means that fewer balls will carry more load.

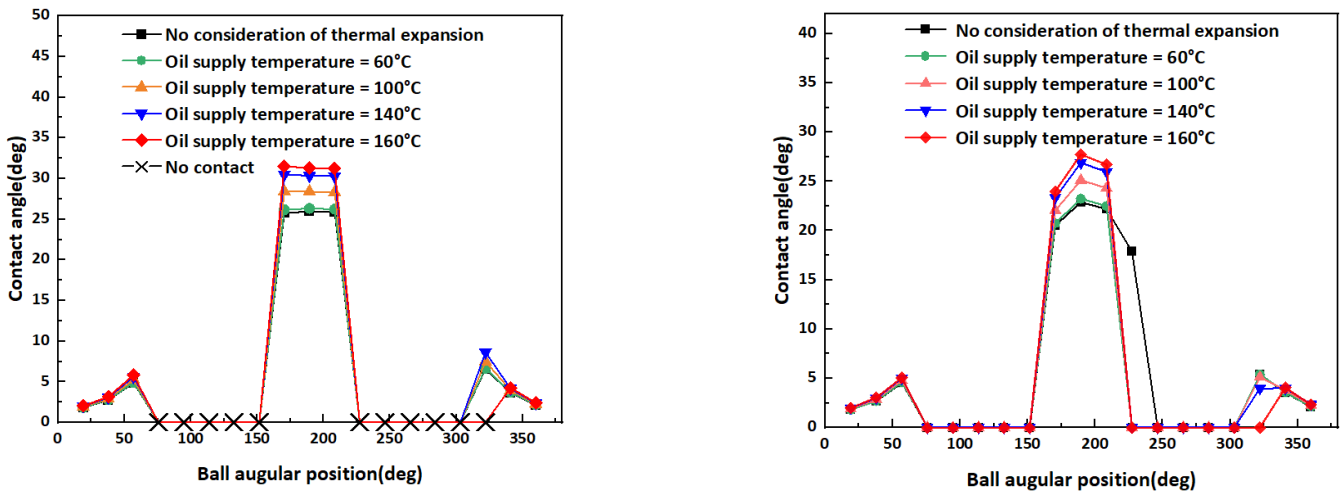


Figure 13. Variation of contact angle.

5.3. Effect of Temperature on Theoretical Fatigue Life

These changes in contact characteristics manifest themselves macroscopically as an effect on fatigue life, and the rated life of a complete set of bearings is estimated by the following equation

$$L_{10} = \left(L_i^{-10/9} + L_o^{-10/9} \right)^{-0.9} \tag{35}$$

$$L_{i,o} = \left(\frac{C_{i,o}}{Q_{i,o}} \right)^3 \tag{36}$$

where L_{10} is in units of 10^6 circles and the point contact rated rolling body load $C_{i,o}$ is obtained from the following formula

$$C_{i,o} = 98.1 \left(\frac{2f_{i,o}}{2f_{i,o} - 1} \right)^{0.41} \frac{(1 \mp \gamma)^{1.39}}{(1 \pm \gamma)^{1/3}} \left(\frac{\gamma}{\cos a_0} \right)^{0.3} D_w^{1.8} Z^{-1/3} \quad (37)$$

In the above equation, the symbols above apply to the inner ring and the symbols below apply to the outer ring. The equivalent rolling body loads are as follows

$$\begin{cases} Q_i = \left(\frac{1}{Z} \sum_{j=1}^Z Q_{ij}^3 \right)^{1/3} \\ Q_o = \left(\frac{1}{Z} \sum_{j=1}^Z Q_{oj}^{10/3} \right)^{3/10} \end{cases} \quad (38)$$

The results of the fatigue life calculation are shown in Figure 14.

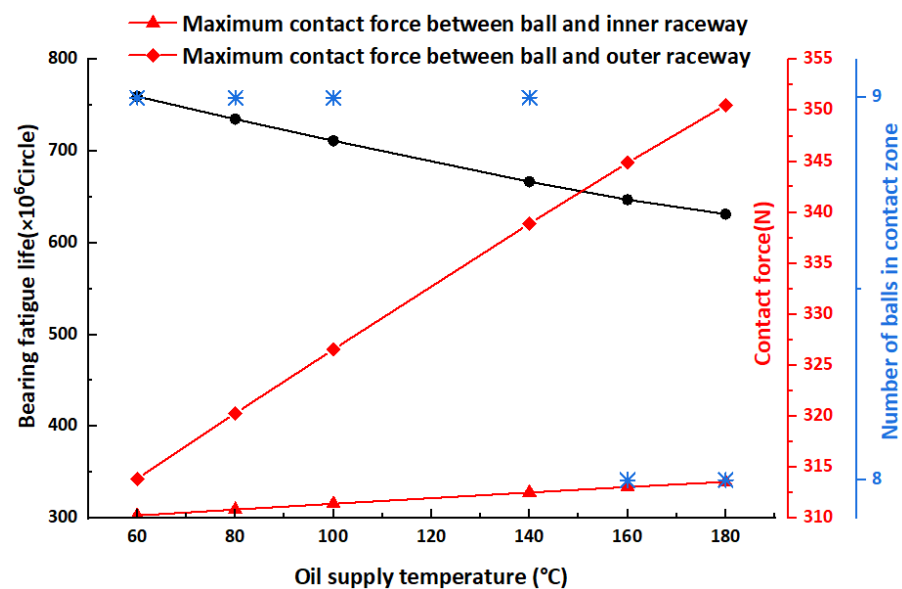


Figure 14. Relationship between contact characteristics and fatigue life.

Combined with Figures 12 and 14, it can be seen that the low fatigue life of bearings working at high temperatures may be due to the fact that the number of loaded rolling elements tends to decrease and the load on rolling elements tends to concentrate. It is not difficult to infer that when the temperature rises sharply, a very small number of balls will bear the full applied load, which will also lead to a thermal seizure.

6. Conclusions

- (1) Under operating conditions of 12,000 rpm, 900 N radial force, and 100 N axial force, the thermal effect of a 100 °C temperature difference increases the maximum contact force by 8% and reduces the theoretical fatigue life by 12%, which cannot be taken into account in purely mechanical analysis.
- (2) Under the action of a strong asymmetric load, the temperature rise will tend to reduce the number of balls in the contact area of the inner raceway.
- (3) The temperature rise tends to concentrate the load distribution, which may be one of the reasons for the reduction in fatigue life.

Author Contributions: Methodology and writing—original draft preparation, Y.D. and F.C.; data processing and mining, editing; M.Q., supervision; H.W. and C.Y., data checking. All authors have read and agreed to the published version of the manuscript.

Funding: This research was funded by the National Key R & D Program of China, grant number 2020YFB2007304, National Natural Science Foundation of China, grant number 52205096, Henan province postdoctoral research, grant number 202002064, the science fund of state key laboratory of tribology, grant number SKLTKF20A03, the Key Research Projects for Higher Education Institutions of Henan Provincial Education Department, grant number 23A460007.

Institutional Review Board Statement: Not applicable.

Informed Consent Statement: Not applicable.

Data Availability Statement: The data sets supporting the results of this article are included within the article.

Conflicts of Interest: The authors declare no conflict of interest.

References

1. Yan, K.; Yan, B.; Wang, Y.; Hong, J.; Zhang, J. Study on thermal induced preload of ball bearing with temperature compensation based on state observer approach. *Int. J. Adv. Manuf. Technol.* **2018**, *94*, 3029–3040. [\[CrossRef\]](#)
2. Palmgren, A. *Ball and Roller Bearing Engineering*; SKF Industries Inc.: Philadelphia, PA, USA, 1959.
3. Harris, T.A.; Kotzalas, M.N. *Advanced Concepts of Bearing Technology: Rolling Bearing Analysis*; CRC Press: London, UK, 2006.
4. Li, Z.; Guan, X.; Zhong, R.; Wang, Q. Analysis of Dynamic Characteristics of Angle Contact Bearings with Combined Load. *J. Mech. Eng.* **2020**, *56*, 116–125.
5. Zhang, J.; Fang, B.; Hong, J.; Zhu, Y. Effect of preload on ball-raceway contact state and fatigue life of angular contact ball bearing. *Tribol. Int.* **2017**, *114*, 365–372. [\[CrossRef\]](#)
6. Zhang, J.; Fang, B.; Zhu, Y.; Yan, K.; Hong, J. Investigation of the Load Distribution and Stiffness Characteristic of Ball Bearing under Ball-raceway Separation Condition. *J. Mech. Eng.* **2020**, *56*, 73–83.
7. Zhang, Q.-Q.; Zhang, C. Thermal Characteristics Analysis and Test of High-speed Angle Contact Ball Bearing for Grease Lubrication. *Sci. Technol. Eng.* **2021**, *21*, 2286–2292.
8. Zhang, C.; Tian, J.; Guo, D.; Niu, Q. Thermal characteristics of grease lubricated high-speed angular contact ball bearings with thermal deformation. *J. Tsinghua Univ. (Sci. Technol.)* **2022**, *62*, 482–492.
9. Yu, J.; Liu, Z.; Shao, J.; He, L.; Yuan, W. Dynamic property of spindle bearing considering the effect of thermal deformation. *J. Aerosp. Power* **2018**, *33*, 477–486.
10. Yan, K.; Hong, J.; Zhang, J.H.; Mi, W.; Wu, W. Thermal-deformation coupling in thermal network for transient analysis of spindle-bearing system. *Int. J. Therm. Sci.* **2016**, *104*, 1–12. [\[CrossRef\]](#)
11. Zheng, D.X.; Chen, W.F.; Li, M.M. An optimized thermal network model to estimate thermal performances on a pair of angular contact ball bearings under oil-air lubrication. *Appl. Therm. Eng.* **2018**, *131*, 328–339.
12. Zheng, D.X.; Chen, W.F. Effect of structure and assembly constraints on temperature of high-speed angular contact ball bearings with thermal network method. *Mech. Syst. Signal Process.* **2020**, *145*, 106929. [\[CrossRef\]](#)
13. Liu, Y.; Ma, Y.X.; Meng, Q.Y.; Xin, X.-C.; Ming, S.-S. Improved thermal resistance network model of motorized spindle system considering temperature variation of cooling system. *Adv. Manuf.* **2018**, *6*, 384–400. [\[CrossRef\]](#)
14. Than, V.T.; Huang, J.H. Nonlinear thermal effects on high-speed spindle bearings subjected to preload. *Tribol. Int.* **2016**, *96*, 361–372. [\[CrossRef\]](#)
15. Xia, Z.X.; Wu, Y.H.; Ma, T.B.; Bao, Z.; Tian, J.; Gao, L.; Sun, J.; Li, S. Experimental study on adaptability of full ceramic ball bearings under extreme conditions of cryogenics and heavy loads. *Tribol. Int.* **2022**, *175*, 107849. [\[CrossRef\]](#)
16. Wang, Y.B.; Yan, C.F.; Lu, Z.Y.; Wu, L. Effect of thermal elastohydrodynamic lubrication on vibration characteristics of ball bearing with local defect. *Proc. Inst. Mech. Eng. Part K-J. Multi-Body Dyn.* **2022**, *236*, 488–500. [\[CrossRef\]](#)
17. Cao, Y.; Altintas, Y. A general method for the modeling of spindle-bearing systems. *J. Mech. Des.* **2004**, *126*, 1089–1104. [\[CrossRef\]](#)
18. Ding, C.; Zhou, F.; Zhu, J.; Zhang, L. Raceway control assumption and the determination of rolling element attitude angle. *Chin. J. Mech. Eng.* **2001**, *37*, 58–61. [\[CrossRef\]](#)
19. Deng, S.; Hua, X.; Zhang, W. Analysis on friction torque fluctuation of angular contact ball bearing in gyro motor. *J. Aerosp. Power* **2018**, *33*, 1713–1724.
20. Takabi, J.; Khonsari, M.M. Experimental testing and thermal analysis of ball bearings. *Tribol. Int.* **2013**, *60*, 93–103. [\[CrossRef\]](#)
21. Crecelius, W.J.; Pirvics, J. *Computer Program Operation Manual on SHABERTH-A Computer Program for the Analysis of the Steady State and Transient Thermal Performance of Shaft-Bearing Systems*; A189240; Engineering and Research Center of SKF Industries: King of Prussia, PA, USA, 1976.